Density of amorphous GeO_2 to 133 GPa with possible pyritelike structure and stiffness at high pressure

Sylvain Petitgirard,[1,*] Georg Spiekermann,[2,†] Konstantin Glazyrin,[3] Jan Garrevoet,[3] and Motohiko Murakami[1]
[1]*Department of Earth Sciences, ETH Zürich, Zürich 8025, Switzerland*
[2]*Institut für Geowissenschaften, Universität Potsdam, 14476 Potsdam, Germany*
[3]*Deutsches Elektronen-Synchrotron DESY, 22607 Hamburg, Germany*

(Received 5 August 2019; revised manuscript received 19 October 2019; published 4 December 2019)

Germanium oxide is a prototype network-forming oxide with pressure-induced structural changes similar to those found in crystals and amorphous silicate oxides at high pressure. Studying density and coordination changes in amorphous GeO_2 allows for insight into structural changes in silicate oxides at very high pressure, with implications for the properties of planetary magmas. Here, we report the density of germanium oxide glass up to 133 GPa using the x-ray absorption technique, with very good agreement with previous experimental data at pressure below 40 GPa and recent calculation up to 140 GPa. Our data highlight four distinct compressibility domains, corresponding to changes of the local structure of GeO_2. Above 80 GPa, our density data show a compressibility and bulk modulus similar to the counterpart crystal phase, and we propose that a compact distorted sixfold coordination, similar to the structural motif of the pyritelike crystalline GeO_2 polymorph, is likely to be stable in that pressure range. Our density data point to a smooth continuous evolution of the average coordination for pressure above 20 GPa with persistent sixfold coordination, without sharp density or density slope discontinuities. These observations are in very good agreement with theoretical calculations and spectroscopic measurements, and our results indicate that glasses and melts may behave similarly to their high-pressure solid counterparts with comparable densities, compressibility, and possibly average coordination.

DOI: 10.1103/PhysRevB.100.214104

I. INTRODUCTION

The relationship between density and structure of amorphous oxides such as SiO_2 and GeO_2 glasses at high pressure is of importance in different fields of research from materials to Earth science and astrophysics. The comprehension of physical properties in condensed amorphous oxides, especially simple oxides (AO_2, with A = Si, Ge, Ti, etc.) is also of high importance for the planetary sciences. SiO_2 is the most abundant component in naturally occurring silicate melts on Earth and other telluric planetary bodies. GeO_2 is a structural analog to SiO_2, being a network former in the amorphous state at ambient pressures and exhibiting a similar succession of crystalline high-pressure structures and transitions, with minor differences only at low pressure [1–6]. At ambient conditions, the structure of both oxides consists of an infinitely extended network of SiO_4^{4-} and GeO_4^{4-} tetrahedra, respectively. Upon compression, the rather loose tetrahedral network transforms to a more compact structure, first with a reduction of intrinsic voids and compaction of the tetrahedron [7], with a distinct quasielastic response below 10 GPa for SiO_2, and a permanent densification above [8,9]. For GeO_2 the permanent densification is achieved almost immediately [10,11]. With the increase in pressure and densification, the number of oxygen neighbors to each localized Si/Ge atom (i.e., the Si or Ge coordination number, CN) increases from four to six through an intermediate fivefold coordination [12–14] that is not easily achieved in the crystalline counterparts and only met under certain experimental circumstances [15]. Higher coordination, with CN > 6, in the compressed glass has been recently claimed [16,17]; however, a consensus has not yet been found whether the glass could be denser than the crystalline structures, when reaching such higher coordination. In this context, quantitative density measurements shed light on how to link the atomic structure arrangement and the macroscopic behavior of glasses and melts [12,18–21]. We emphasize that density measurements are of prime importance for the discussion of macroscopic properties of such materials with application to planetary interiors and solid state physics.

Unresolved is the issue of the density contrast between melts and crystals controlling the buoyancy and fate of melts in planetary interiors [22] and, thus, it limits our understanding of their internal evolution [23,24]. At lower pressures, the density difference between the lighter melts and the heavier minerals is responsible for the chemical differentiation of the Earth's crust from the mantle. If the reverse mechanism would exist at the extreme pressures of the lowermost mantle, then this could provide additional arguments or even fully resolve the discussion for the origin of seismic anomalies at the core-mantle boundary [25,26], with magma accumulation at the top of the core-mantle boundary. Unfortunately, *in situ* density measurements of amorphous magmalike material (dense liquid) at conditions prevailing in planetary interiors remain a severe obstacle. However, it was indicated that amorphous

*Sylvain.Petitgirard@erdw.ethz.ch
†geospiek@uni-potsdam.de

SiO_2 and GeO_2 (at ambient temperature and high pressure) have structures similar to the molten states at high depths [13,19,20,27], and, in a first approximation, can be used to infer the behavior of the melt.

The density increase in compressed amorphous oxides, determined by tracking volumetric changes, goes along with changes of their atomic scale structure (cation-anion distances and average coordination), which can be probed by several x-ray techniques, such as x-ray total scattering data (x-ray diffraction, XRD) [17,19,27,28] and x-ray absorption spectroscopy (XAS) [10] or x-ray Raman spectroscopy (XRS) [12,14], x-ray emission spectroscopy through the valence-to-core emission (vtc-XES) [18], and indirectly by optical spectroscopy techniques [29–32]. A general consensus has been reached on the pressure range of the transition from a tetrahedral coordination with CN = 4 to a closest-packed octahedral structure with CN = 6. In SiO_2 this transformation to CN $\sim$ 6 is completed at about 40–60 GPa [12,13,27,33]. For GeO_2, the transition from CN = 4 to CN = 6 takes place between 0 and $\sim$12 GPa, documented by a variety of techniques like XAS [10,11,34], XRS [14], XES [18], x-ray total scattering (XRD), and neutron diffraction [16,35–39].

At higher pressures, the picture concerning the average coordination number (CN) in SiO_2 and GeO_2 remains ambiguous. While it has been claimed recently that the average coordination in SiO_2 may exceed 6 already above 60 GPa [17], another recent report did not observe any evidence for a rise of the average coordination above 6 below 140 GPa [12]. Sound velocities from Brillouin spectroscopy measurements suggest that a change in density, which could be related to higher coordination, may take place only above 140 GPa [29], also proposed by a combination of total scattering data and calculation [40]. From direct density measurements, there is no evidence for a density crossover between the glass and the sixfold crystalline polymorphs up to 110 GPa [20]. This points to a similar evolution of CN and densities with pressure in glasses and their corresponding crystalline solids.

In the case of GeO_2, results diverge even more. On one hand, recent x-ray total scattering data (XRD) proposed a sharp increase in coordination of Ge beyond 6, with CN = 6.5 at 50 GPa and CN > 7 at 90 GPa [16]. On the other hand, a recent x-ray emission spectroscopy (XES) [18] study observed a plateau of CN = 6 up to 100 GPa, while *ab initio* molecular dynamic (AIMD) calculations [41] show a gradual increase of the CN above 6 only starting at 80 GPa, reaching CN = 6.5 for pressure beyond 120 GPa. Finally, the only existing density study for amorphous GeO_2 (a-GeO_2) up to 55 GPa suggests a possible density crossover at 50 GPa [11], but this remains elusive because of a lack of data at high pressure to conclude on such crossover.

Direct measurements of the density of GeO_2 at high pressure are thus missing to complement the measurements and discussion on the atomic scale structure and link the microstructure to the macrostructure evolution. From direct density measurements, we can delimit pressure domains where a uniform equation of state (EOS) fit can be performed to model the data. The transitions between such domains may be attributed to possible changes in the compaction mechanism or an increase in coordination number (CN).

Here we measured the density of amorphous GeO_2 (a − GeO_2) using the x-ray absorption methods up to 133 GPa, more than doubling the pressure range of previous experimental measurements. We found very good agreement between our density data and previous experimental work at low pressure below 45 GPa [11], and also with recent AIMD calculation [41]. Above this pressure, our data deviate from the former data set with lower densities, while being slightly denser than the calculated densities from AIMD. At about 65 GPa our density data slightly exceed, or equal those of the crystalline high-pressure PbO_2 polymorph, but fall back below the density of the pyrite-type $Ge O_2$ at a pressure of 80 GPa and beyond.

II. MEASUREMENTS PROCEDURE AND DATA ANALYSIS

The GeO_2 glass was synthetized in a furnace at T of 1000 °C, followed by rapid quenching of the Pt crucible in water. A bubble-free transparent piece of glass was either double polished to a $\sim$15-μm-thick plate for low-pressure runs or ground into a fine powder for high-pressure measurements. The density measurements were conducted at the P06 beamline in DESY (Hamburg, Germany). The beam was set at 15 keV by a double Si (111) channel cut monochromator and focused to $0.2 \times 0.2\ \mu m^2$ using compound refractive lenses. Samples were loaded in beryllium gaskets in BX90 diamond cells [42] equipped with 350-μm diamonds for low pressure and 250- or 150-μm with 300-μm bevel diamonds for higher pressures. For the low-pressure runs (Fig. 1), glass pieces with sharp edges from the double-polished plate were selected and immersed in methanol:ethanol (4:1) together with a ruby sphere used as a pressure gauge [43]. For the high-pressure run (Fig. S1; see Supplemental Material [44]), the sample chamber in the Be gasket was filled with a powder sample and the Raman shift of the stretching line of the diamond tip was used to measure the pressure [45].

The measurement follows the same procedure as described for $MgSiO_3$ [22] and SiO_2 [20] glass with 2D mapping of the sample under two orientations: (i) through the diamond to obtain the path length (x) of the x rays through the GeO_2 sample (Figs. 1(a) and 1(b) and Figs. S1(a) and S1(b) in the Supplemental Material [44]) and (ii) through the Be gasket in order to measure the x-ray attenuation (I/I_0) of GeO_2 glass under pressure [Figs. 1(c) and 1(d) and Figs. S1(c) and 1(d); see Supplemental Material [44]). The edges of the sample, defining the path length (x), can be obtained with a precision better than 2 μm, corresponding to uncertainty of less than 2% on the density. At very pressure, this increases to about 5%. The absorbance (μ_{HP}) of the sample was extracted from the correlation between the x-ray attenuation and the path length of the sample obtained from both maps (Fig. 1(e) and Figs. S1(e) and S2, in the Supplemental Material [44]). The slope of the linear regression gives the linear absorbance at high pressure (μ_{HP}) through the Beer-Lambert relation:

$$\ln(I/I_0) = -\mu_{HP} x. \quad (1)$$

The density at high pressure (ρ_{HP}) was then calculated by

$$\rho_{HP}/\mu_{HP} = \rho_0/\mu_0. \quad (2)$$

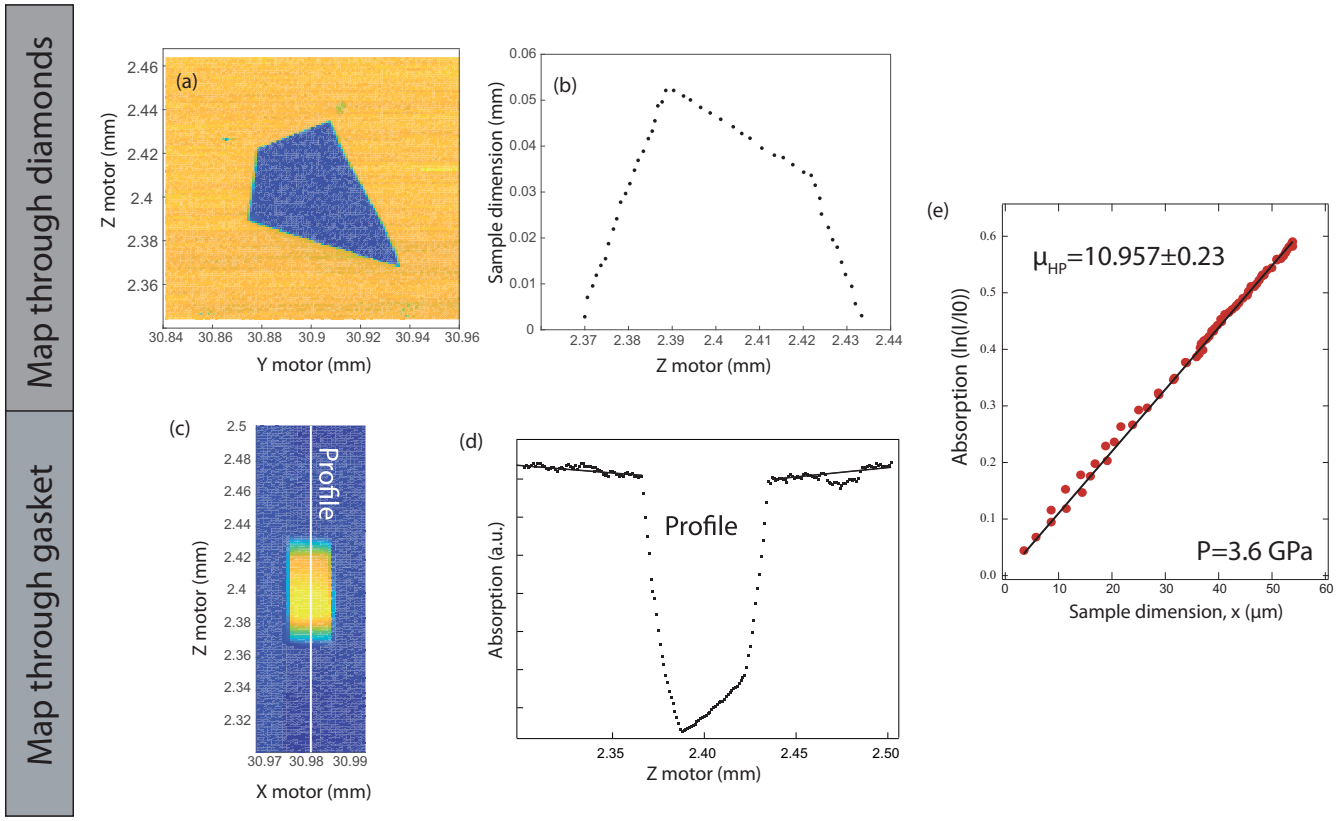

FIG. 1. Data collection scheme inside the DAC, here in a low-pressure run with a double-polished GeO_2 plate immersed in a methanol:ethanol mixture. (a) Map through the diamonds from which the sample's dimensions are determined (b). (c) Absorption map through the Be gasket. (d) A profile extracted from the map. (e) Correlation between (b) and (d) to derive the linear absorbance of the sample, further used to calculate the density at HP.

The attenuation coefficient at ambient pressure (μ_0) was determined from the absorption of a double-polished plate of GeO_2 using the same setup on the beamline, and the ambient pressure density (ρ_0) of 3.506 ± 0.008 g/cm^3.

III. RESULTS AND COMPARISON WITH PREVIOUS REPORTS

Our density data as a function of pressure (Table S1; see Supplemental Material [44]) are reported in Fig. 2 and compared with previous measurements carried out using the x-ray absorption method [11], tomography imaging [46], or AIMD calculation [41], as well as with the density of the crystalline high-pressure GeO_2 polymorphs [1]. The compressibility of GeO_2 can be analyzed using a finite strain plot in the Vinet form [47], or f-F plot, to reveal the different pressure domains of dominant coordination species for which individual equations of state can be derived, as it was shown for the compressed amorphous SiO_2 [20]. For a-GeO_2, at least four compressibility domains can be identified, that may be related to four different atomic configurations of Ge in the glass under pressure. As discussed in previous studies [11,14,48], three domains can be separated at low pressure between 0 and 12 GPa that correspond to the transition from fourfold $^{[4]}$Ge to sixfold $^{[6]}$Ge, with an intermediate domain between 4.5 and 9.8 GPa that possibly contains $^{[5]}$Ge species as identified by fingerprints and distinct changes in the O K edge using x-ray Raman spectroscopy [14]. Our data clearly indicate a fourth domain above 80 GPa (Fig. 3) and allow to constrain

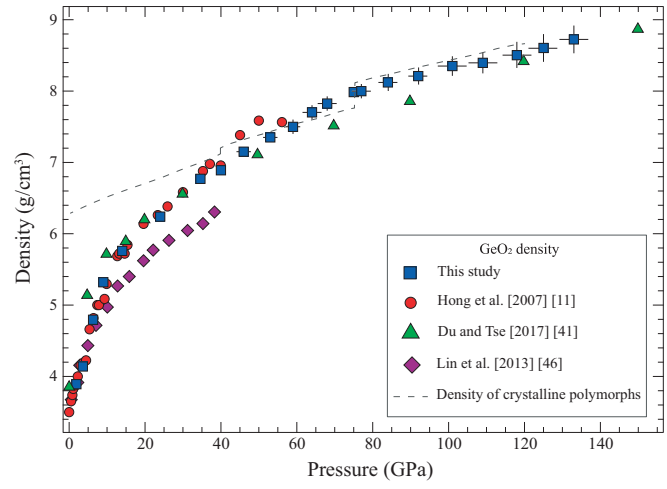

FIG. 2. Density results for a-GeO_2 (squares, this study) compared to other experimental and modeling data. Data from Hong *et al.*, (2007) [11] (circles) measured using the absorption method; data from x-ray tomography, Liu *et al.*, (2013) [46] (diamonds) and triangles; data calculated with *ab initio* calculation, Du and Tse, (2017) [41]. Black dashed line represents the value for the density of the crystals GeO_2, Dutta *et al.*, (2018) [1].

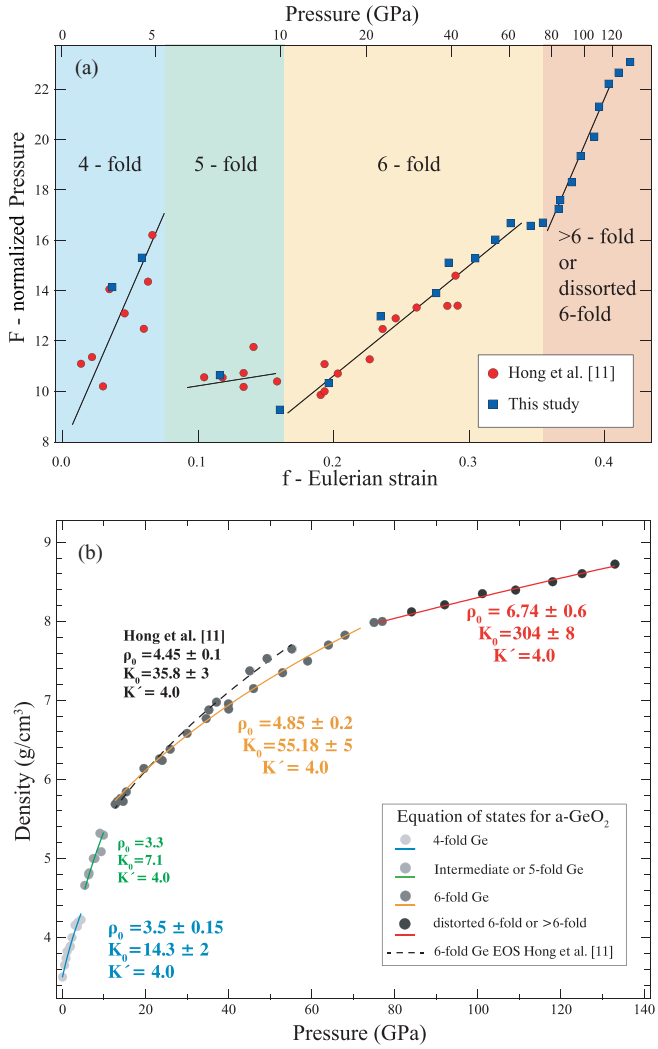

FIG. 3. (a) f-F plot revealing the different compressibility domains with a domain above 80 GPa that could be linked to a sixfold distorted environment for Ge as in the pyrite structure or it may be the start of a higher coordination. (b) Equation of state fits for the different domains.

two EOSs for sixfold coordinated $^{[6]}$Ge below and above 80 GPa. We can provide a revised EOS for the pressure domain between 10 and 80 GPa compared to previous data [11]: with values of $V_0 = 21.25(1)\,\mathrm{cm}^{-3}/\mathrm{mol}$ and $K_0 = 55.2$ (5) GPa, when fixing K_0' to 4 (other parameters can be found when using different values for K_0'; see Table S2 in the Supplemental Material [44]). When extrapolating the EOS reported by Hong *et al.* [11] to higher pressure, we found an overestimation of the density of about 5% and 10% at 50 and 95 GPa, respectively, compared to our data. Such a deviation of the extrapolated density, across the transition at 80 GPa, may be a source of overestimation in the average coordination number (CN) calculation when using the x-ray total scattering method [16]. At 80 GPa, the compressibility in our study shows a clear change with a kink in the f-F plot [Fig. 3(a)], with a saturation of the density at higher pressure being asymptotic to the one of the crystalline pyritelike structure (Fig. 2). At such pressure the material has a high bulk modulus of about 300 GPa, derived from our third-order BM fit ($V_0 = 15.39(1.5)\,\mathrm{cm}^{-3}/\mathrm{mol}$, $K_0 = 304$ (8) GPa and $K_0' = 4$, Table S2; see Supplemental Material [44]), almost similar to the one of the crystalline GeO_2 in the pyrite structure, with $K_0 = 347$ (12) GPa ($K_0' = 4$) [1] and also equivalent to the one of the α-PbO_2 structure with $K_0 = 292$ (10) GPa ($K_0' = 4$). At higher pressure, the propagated values for the bulk modulus will also be comparable between the crystalline and amorphous phases, because of the similarity in the parameters for the EOS (same K' values). The a-GeO_2 becomes very stiff at such pressure, comparable to the crystalline structure, indicating a very similar behavior of the amorphous and crystalline states at very high pressure.

At 80 GPa, we do not observe an increase in density nor a drastic change in compressibility, which rather follows a smooth trend. In the f-F plot, there is almost a continuous change below and above 80 GPa. We interpret this smooth change in compressibility as a transition to a more compact distorted structure but we do not rule out a potential proportion of higher coordinated Ge at such pressure. The bulk modulus of the amorphous phases at high pressures approaches that of the counterpart crystalline structure [$K_0 = 304$ (8) GPa for a-GeO_2 compared to $K_0 = 347$ (12) GPa for the pyrite structure which has a sixfold coordinated structure] indicating that the compressibility is almost the same between the two compounds. Indeed, at such high pressure the compaction of the structure is dominated by bond shortening, or rotation of the octahedron [49,50], and coordination change is less likely.

IV. DISCUSSION

The change in compressibility in a-GeO_2 around 80 GPa is of special interest, as two contradictory coordination evolution paths have been suggested in this pressure range: A change to sevenfold coordination [41] or a distortion of sixfold octahedron [18]. Indeed, a distortion, or rotation, of the GeO_2 octahedrons can bring oxygen atoms closer to the Ge atoms (bond shortening), without necessarily increasing the CN above 6, as is the case in the crystalline structure evolution from rutile to $CaCl_2$ to α-PbO_2 to the pyrite structure [51]. The persistence of sixfold coordination in a-GeO_2 was recently reported using x-ray emission spectroscopy (XES) that enables probing electrons in the orbitals directly involved in the bonding between germanium and oxygen [18]. This approach has not reported any sign of an increase in coordination. It even demonstrates that the atomic Ge-O distances extracted from XES are very similar to the one obtained from XRD [16], XAS at lower pressure [10], and also comparable to AIMD calculation [41]. The XES measurements show a flattening of the Ge-O distances at a pressure corresponding to the density crossover measured in our study and at higher pressure the Ge-O distance decreases following a monotonous trend with no sign of a sharp change, very close to Ge-O distances measured in the crystal structures. This suggests that a succession of distortion of octahedral sites, while keeping a sixfold coordination, is a more favorable mechanism in the glass than an increase of coordination, and mimics the changes measured in the crystal structures.

The compressibility changes as a function of pressure that we report here bring important information for the coordina-

tion evolution in a-GeO_2 by comparing the densities and bulk modulus to the one of the crystalline phases. In the pressure regime between 0 and 12 GPa, the changes from $^{[4]}$Ge to $^{[5]}$Ge and to $^{[6]}$Ge in a-GeO_2 seem to be accompanied with a sharp increase in density between each domain, almost like a first-order transition would look like. This is also quite noticeable in the f-F plot with clear changes between the compressibility of the different domains. The evolution of the bulk modulus is also remarkable with a fourfold increase from the $^{[4]}$Ge a-GeO_2 to the $^{[6]}$Ge a-GeO_2 (Table S2; see Supplemental Material [44]). However, from density data solely it is difficult to directly determine the coordination of Ge in the glass.

The subtle density crossover we measured can thus be explained with an overlap, or coexistence, of a-GeO_2 local environments during the conversion of the sixfold CN from the α-PbO_2 structure to the distorted sixfold pyritelike structure. We expect that the change from the two types of structure takes place gradually in the glass as the two crystalline units are quite similar. While in the crystalline structures this change in structure goes with a density change of about 4%–5%, the glass can accommodate this density jump by gradually changing from CN = 6 of the α-PbO_2 structure to the distorted sixfold FeS_2 structure, with a mixture of structures between 65 and 80 GPa. Hence, a density crossover happens in a-GeO_2 due to a mixture of low-density sixfold and a higher-density distorted sixfold coordination before reaching almost a similar density as the crystalline FeS_2 structure above 80 GPa (Fig. 2), after the completion of the structural change.

Our analysis helps to reveal additional details on the behavior of a-GeO_2 at lower pressure from 15 to 80 GPa. In this range, the crystalline phases undergo several transitions from rutile-type to $CaCl_2$ to α-PbO_2 (all sixfold CN), but without noticeable change in the density for the amorphous phase (Fig. 2), as if the glass was insensitive to such transitions. The amorphous phase can easily accommodate a mixture of close local structures for Ge (all being sixfold), thus making the density trend much smoother compared to the one measured in the crystalline sequence. On the contrary, below 10 GPa, when a clear change in coordination occurs, it induces a drastic change in density (Fig. 2), bulk modulus, and compressibility when passing from four- to sixfold coordination (Figs. 2 and 3). All our data, density, and bulk modulus yield the same conclusion: At very high pressure these properties in the glass and the crystalline structure are similar; thus their atomic structure is very likely to be similar. As discussed for SiO_2, it seems then odd that the glass structure could reach higher coordination than the solid while the density remains somehow lower or equal [12,18,20,21,33]. Knowledge of the relationship between the density, bulk modulus, and microstructure in the amorphous and crystalline phase is thus a key for the comprehension of the evolution of CN in the amorphous material. Higher coordination in the crystalline structure is reported to take place at much higher pressure upon the transition from pyrite (FeS_2, CN = 6) to cotunnite (α-$PbCl_2$, CN = 9) at 280 GPa for GeO_2 [51] and more than 700 GPa for SiO_2 [52]. Unfortunately, there are no experimental data available for such conditions. However, TiO_2 is a related system, with structural changes similar to SiO_2 and GeO_2 at lower pressures, with a transition from a sixfold pyrite structure to a ninefold cotunnite structure at 60 GPa [53]. This transition in TiO_2 is marked with a possible increase in the bulk modulus up to 480 GPa [54,55] and a noticeable volume collapse of few percent [53,55]. Thus, we anticipate that the change in CN in a-GeO_2 to higher coordination should be linked to a steep change in density and bulk modulus for P beyond 280 GPa, similar to the density changes in the low-pressure domain when converting $^{[4]}$Ge to $^{[6]}$Ge.

The extreme packing of the a-GeO_2 structure at high pressure induces a high electron density in a very short distance resulting from the Ge-O and O-O coordination, such that it may not be easily deconvoluted in a radial distribution function analysis. This points out the need for further work in this domain to improve the resolution from such data and to avoid contributions from other close neighboring atoms. Such a phenomenon was already reported for SiO_2 glass, with electrons of the O-O bond interacting with the Si-O electrons distribution peak due to insufficient resolution in the radial distribution function (RDF) at extreme pressure [17]. This becomes problematic for more complex structures rendering impossible to resolve cation-oxide distances that are too close from one another, for instance, Si-O and Mg-O in $MgSiO_3$ [56], precluding conclusions on coordination changes of any of the cations of more complex compositions. The difficulty to resolve bonded electrons and electrons from very close neighboring atoms can be at the origin of the overestimation of CN when using XRD as a probe and requires a combined approach investigating the bulk material behavior through density analysis as well as element sensitive techniques such as XRS or XES but also using AIMD calculation. To date there is still no experimental spectroscopic evidence or a clear fingerprint for higher coordination of Ge in a-GeO_2. An investigation at the oxygen K edge using XRS may bring some fingerprints indicating differences in coordination compared to the sixfold, as it was measured at low pressure to identify a fivefold Ge in a-GeO_2 [14]. This would require dedicated measurements of the O K edge combined with a computational approach to obtain structures from which spectra can be calculated and compared with [12,14]. Still, as we show here, the comparison of densities and bulk modulus between amorphous and crystalline phases can bring important evidence of the similarities between the physical properties of the amorphous and crystalline phases at high pressure.

V. CONCLUSION

Finally, similar to SiO_2, but unlike the more depolymerized $MgSiO_3$ [22], the compression curve for GeO_2 displays distinct pressure domains. Such a behavior of highly polymerized network-forming oxides indicates kinetic hindrance and can explain the slight difference in densities observed between the cold compressed glass and quenched melts from calculations, for both SiO_2 and GeO_2, especially at pressures at which a compressibility change is observed in the f-F plot, i.e., where structural changes occur at around 10 and 80 GPa. The addition of cation modifiers, such as Mg, lowers kinetic barriers and therefore allows less polymerized structures to achieve better agreement between measured density of glass between the cold compressed $MgSiO_3$ [22] and the one computed in AIMD from quench melt [21]. Thus, the experimental

densities of intermediate polymerized glass, such as naturally occurring melt composition with different cation-network modifiers, e.g., basalt or pyrolite, will be of great interest for planetary interiors, as lowered kinetic barriers result in a melt-like compression path for the glass. Experimental compression curves could then be representative of the compression curve of the melt at high pressure and temperature.

To conclude, we measured the density of amorphous GeO_2 up to 133 GPa and identified four compressibility domains in this pressure range. Up to 45 GPa, our data are in excellent agreement with previous data as well as with calculations from AIMD. Above 45 GPa, we measured densities lower than previous experimental results over a wider pressure range and found a different equation of state for a sixfold coordinated trend between 12 and 80 GPa. This leads to a difference in density of 5% and up to 10% between 55 and 95 GPa, respectively, when extrapolating the previous EOS, and may be one of the reasons for the overestimation of CN beyond 6 from a former report using the total x-ray scattering method [16]. Our analysis shows that $^{[6]}$Ge is the dominant species over the entire pressure range above 15 GPa although we observe a density crossover at 65 GPa. Above 80 GPa, we report a compressibility change that can be fitted with a single EOS up to 133 GPa. Our data show an increase in the stiffness of the material with a bulk modulus of $K_0 =$ 304 (8) GPa, five times higher than the lower-pressure EOS and very close to the sixfold distorted pyritelike octahedral crystal structure that is stable in this pressure domain. This change in compressibility of a-GeO_2 with a stiffening of the material can be related to the distortion and compaction of $^{[6]}$Ge octahedral sites [18]; however, we cannot rule out a possible increase in coordination from density data solely. The combination of density measurements on amorphous material, with changes in compressibility, and other spectroscopic probes likes XES or XANES, can help to infer the structural and coordination evolution with pressure. While coordination higher than sixfold is likely to take place in oxide glass and melts at extreme pressure [57], our density data show a rather continuous change with pressure and there is no indication of a sudden increase in density, thus in coordination, at 55 GPa. We did not find evidence for coordinated sevenfold $^{[7]}$Ge, although some high-coordinated Ge can be formed above 80 GPa. Further experiments should be carried out on both oxygen and germanium electronic structure to shed new light on the coordination environment between the two atoms. The combination of methods and approaches is the only way to provide information about coordination and structure in high-density oxide glasses. However, a common trend arises with densities of glasses being always lower, or almost similar, to their counterpart solids at very high pressure [20–22,58]. It implies that density crossover between solid and liquid will not take place in an isochemical scenario [59] and partitioning of elements, especially iron, will play a major role in the buoyancy of melts and formation of deep magma oceans [24,60,61].

ACKNOWLEDGMENTS

We are particularly grateful to R. Njul from BGI, for the polishing of the starting samples prior to the beam time. We are grateful to M. Wilke and M. Krstulovic for providing the GeO_2 starting material. We are thankful to H. P. Liermann and Extreme Conditions Science Infrastructure of Petra III for the access and use of the off-line Raman system of beamline P02.2. We acknowledge DESY (Hamburg, Germany), a member of the Helmholtz Association HGF, for the provision of experimental facilities. Parts of this research were carried out at the Petra III beamline P06. The research leading to this result has been supported by the project CALIPSOplus under the Grant Agreement No. 730872 from the EU Framework Programme for Research and Innovation HORIZON 2020.

[1] R. Dutta, C. E. White, E. Greenberg, V. B. Prakapenka, and T. S. Duffy, Equation of state of the α-PbO_2 and $Pa\bar{3}$-type phases of GeO_2 to 120 GPa, Phys. Rev. B **98**, 144106 (2018).

[2] J. Haines, J. M. Leger, C. Chateau, and A. S. Pereira, Structural evolution of rutile-type and $CaCl_2$-type germanium dioxide at high pressure, Phys. Chem. Miner. **27**, 575 (2000).

[3] J. Haines, J. M. Léger, and C. Chateau, Transition to a crystalline high-pressure phase in α-GeO_2 at room temperature, Phys. Rev. B **61**, 8701 (2000).

[4] K. Shiraki, T. Tsuchiya, and S. Ono, Structural refinements of high-pressure phases in germanium dioxide, Acta Crystallogr., Sect. B **59**, 701 (2003).

[5] S. Ono, K. Hirose, N. Nishiyama, and M. Isshiki, Phase boundary between rutile-type and $CaCl_2$-type germanium dioxide determined by *in situ* x-ray observations, Am. Mineral. **87**, 99 (2002).

[6] S. Ono, T. Tsuchiya, K. Hirose, and Y. Ohishi, High-pressure form of pyrite-type germanium dioxide, Phys. Rev. B **68**, 014103 (2003).

[7] A. N. Clark, C. E. Lesher, S. D. Jacobsen, and S. Sen, Mechanisms of anomalous compressibility of vitreous silica, Phys. Rev. B **90**, 174110 (2014).

[8] C. Meade and R. Jeanloz, Frequency-dependent equation of state of fused silica to 10 GPa, Phys. Rev. B **35**, 236 (1987).

[9] T. Deschamps, J. Margueritat, C. Martinet, A. Mermet, and B. Champagnon, Elastic moduli of permanently densified silica glasses, Sci. Rep. **4**, 7193 (2014).

[10] X. Hong, M. Newville, T. S. Duffy, S. R. Sutton, and M. L. Rivers, X-ray absorption spectroscopy of GeO_2 glass to 64 GPa, J. Phys.: Condens. Matter **26**, 035104 (2014).

[11] X. Hong, G. Shen, V. B. Prakapenka, M. L. Rivers, and S. R. Sutton, Density measurements of noncrystalline materials at high pressure with diamond anvil cell, Rev. Sci. Instrum. **78**, 103905 (2007).

[12] S. Petitgirard, C. J. Sahle, C. Weis, K. Gilmore, G. Spiekermann, J. S. Tse, M. Wilke, C. Cavallari, V. Cerantola, and C. Sternemann, Magma properties at deep Earth's conditions from electronic structure of silica, Geochem. Perspect. Lett. **9**, 32 (2019).

[13] M. Wu, Y. Liang, J.-Z. Jiang, and J. S. Tse, Structure and properties of dense silica glass, Sci. Rep. **2**, 398 (2012).

[14] G. Lelong, L. Cormier, G. Ferlat, V. Giordano, G. S. Henderson, A. Shukla, and G. Calas, Evidence of fivefold-coordinated Ge atoms in amorphous GeO_2 under pressure using inelastic x-ray scattering, Phys. Rev. B **85**, 134202 (2012).

[15] E. Bykova, M. Bykov, A. Cernok, J. Tidholm, S. I. Simak, O. Hellman, M. P. Belov, I. A. Abrikosov, H.-P. Liermann, M. Hanfland, V. B. Prakapenka, C. Prescher, N. Dubrovinskaia, and L. Dubrovinsky, Metastable silica high pressure polymorphs as structural proxies of deep Earth silicate melts, Nat. Commun. **9**, 4789 (2018).

[16] Y. Kono, C. Kenney-Benson, D. Ikuta, Y. Shibazaki, Y. Wang, and G. Shen, Ultrahigh-pressure polyamorphsim in GeO_2 glass with coordination number >6, Proc. Natl. Acad. Sci. USA **113**, 3436 (2016).

[17] C. Prescher, V. B. Prakapenka, J. Stefanski, S. Jahn, L. B. Skinner, and Y. Wang, Beyond sixfold coordinated Si in SiO_2 glass at ultrahigh pressures, Proc. Natl. Acad. Sci. USA **114**, 10041 (2017).

[18] G. Spiekermann, M. Harder, K. Gilmore, P. Zalden, C. J. Sahle, S. Petitgirard, M. Wilke, N. Biedermann, C. Weis, W. Morgenroth, J. S. Tse, E. Kulik, N. Nishiyama, H. Yavas, and C. Sternemann, Persistent Octahedral Coordination in Amorphous GeO_2 up to 100 GPa by $K\beta''$ X-Ray Emission Spectroscopy, Phys. Rev. X **9**, 011025 (2019).

[19] C. Sanloup, J. W. Drewitt, Z. Konopkova, P. Dalladay-Simpson, D. M. Morton, N. Rai, W. Van Westrenen, and W. Morgenroth, Structural change in molten basalt at deep mantle conditions, Nature **503**, 104 (2013).

[20] S. Petitgirard, W. J. Malfait, B. Journaux, I. E. Collings, E. S. Jennings, I. Blanchard, I. Kantor, A. Kurnusov, M. Cotte, T. Dane, M. Burghammer, and D. C. Rubie, SiO_2 Glass Density to Lower-Mantle Pressures, Phys. Rev. Lett. **119**, 215701 (2017).

[21] D. B. Ghosh, B. B. Karki, and L. Stixrude, First-principles molecular dynamics simulations of $MgSiO_3$ glass: Structure, density, and elasticity at high pressure, Am. Mineral. **99**, 1304 (2014).

[22] S. Petitgirard, W. J. Malfait, R. Sinmyo, I. Kupenko, L. Hennet, D. Harries, T. Dane, M. Burghammer, and D. C. Rubie, Fate of $MgSiO_3$ melts at core-mantle boundary conditions, Proc. Natl. Acad. Sci. USA **112**, 14186 (2015).

[23] S. Labrosse, J. W. Hernlund, and N. Coltice, A crystallizing dense magma ocean at the base of the Earth's mantle, Nature **450**, 866 (2007).

[24] R. Caracas, K. Hirose, R. Nomura, and M. D. Ballmer, Melt-crystal density crossover in a deep magma ocean, Earth Planet. Sci. Lett. **516**, 202 (2019).

[25] M. D. Ballmer, C. Houser, J. W. Hernlund, R. M. Wentzcovitch, and K. Hirose, Persistence of strong silica-enriched domains in the Earth's lower mantle, Nat. Geosci. **10**, 236 (2017).

[26] E. J. Garnero, A. K. McNamara, and S.-H. Shim, Continent-sized anomalous zones with low seismic velocity at the base of Earth's mantle, Nat. Geosci. **9**, 481 (2016).

[27] T. Sato and N. Funamori, High-pressure structural transformation of SiO_2 glass up to 100 GPa, Phys. Rev. B **82**, 184102 (2010).

[28] C. Meade, R. J. Hemley, and H. K. Mao, High-Pressure X-Ray Diffraction of SiO_2 Glass, Phys. Rev. Lett. **69**, 1387 (1992).

[29] M. Murakami and J. D. Bass, Spectroscopic Evidence for Ultrahigh-Pressure Polymorphism in SiO_2 Glass, Phys. Rev. Lett. **104**, 025504 (2010).

[30] C. S. Zha, R. J. Hemley, H. K. Mao, T. S. Duffy, and C. Meade, Acoustic velocities and refractive index of SiO_2 glass to 57.5 GPa by Brillouin spectroscopy scattering, Phys. Rev. B **50**, 13105 (1994).

[31] R. J. Hemley, H. K. Mao, P. M. Bell, and B. O. Mysen, Raman Spectroscopy of SiO_2 Glass at High Pressure, Phys. Rev. Lett. **57**, 747 (1986).

[32] S.-H. Shim and K. Catalli, Compositional dependence of structural transition pressures in amorphous phases with mantle-related compositions, Earth Planet. Sci. Lett. **283**, 174 (2009).

[33] B. B. Karki, D. Bhattarai, and L. Stixrude, First-principles simulations of liquid silica: Structural and dynamical behavior at high pressure, Phys. Rev. B **76**, 104205 (2007).

[34] M. Vaccari, G. Aquilanti, S. Pascarelli, and O. Mathon, A new EXAFS investigation of local structural changes in amorphous and crystalline GeO_2 at high pressure, J. Phys.: Condens. Matter **21**, 145403 (2009).

[35] M. Guthrie, C. A. Tulk, C. J. Benmore, J. Xu, J. L. Yarger, D. D. Klug, J. S. Tse, H. K. Mao, and R. J. Hemley, Formation and Structure of a Dense Octahedral Glass, Phys. Rev. Lett. **93**, 115502 (2004).

[36] Q. Mei, S. Sinogeikin, G. Shen, S. Amin, C. J. Benmore, and K. Ding, High-pressure x-ray diffraction measurements on vitreous GeO_2 under hydrostatic conditions, Phys. Rev. B **81**, 174113 (2010).

[37] J. A. E. Desa, A. C. Wright, and R. N. Sinclair, A neutron-diffraction investigation of the structure of vitreous germania, J. Non-Cryst. Solids **99**, 276 (1988).

[38] J. W. E. Drewitt, P. S. Salmon, A. C. Barnes, S. Klotz, H. E. Fischer, and W. A. Crichton, Structure of GeO_2 glass at pressures up to 8.6 GPa, Phys. Rev. B **81**, 014202 (2010).

[39] P. S. Salmon, J. W. E. Drewitt, D. A. J. Whittaker, A. Zeidler, K. Wezka, C. L. Bull, M. G. Tucker, M. C. Wilding, M. Guthrie, and D. Marrocchelli, Density-driven structural transformations in network forming glasses: A high-pressure neutron diffraction study of GeO_2 glass up to 17.5 GPa, J. Phys.: Condens. Matter **24**, 439601 (2012).

[40] M. Murakami, S. Kohara, N. Kitamura, J. Akola, H. Inoue, A. Hirata, Y. Hiraoka, Y. Onodera, I. Obayashi, J. Kalikka, N. Hirao, T. Musso, A. S. Foster, Y. Idemoto, O. Sakata, and Y. Ohishi, Ultrahigh-pressure form of SiO_2 glass with dense pyrite-type crystalline homology, Phys. Rev. B **99**, 045153 (2019).

[41] X. P. Du and J. S. Tse, Oxygen packing fraction and the structure of silicon and germanium oxide glasses, J. Phys. Chem. B **121**, 10726 (2017).

[42] I. Kantor, V. Prakapenka, A. Kantor, P. Dera, A. Kurnosov, S. Sinogeikin, N. Dubrovinskaia, and L. Dubrovinsky, BX90: A new diamond anvil cell design for x-ray diffraction and optical measurements, Rev. Sci. Instrum. **83**, 125102 (2012).

[43] A. Dewaele, M. Torrent, P. Loubeyre, and M. Mezouar, Compression curves of transition metals in the Mbar range: Experiments and projector augmented-wave calculations, Phys. Rev. B **78**, 104102 (2008).

[44] See Supplemental Material at http://link.aps.org/supplemental/10.1103/PhysRevB.100.214104 for information about high pressure denisty data acquisitions, a table with all density data, and a table with different EOS fits.

[45] Y. Akahama and H. Kawamura, Pressure calibration of diamond anvil Raman gauge to 310 GPa, J. Appl. Phys. **100**, 043516 (2006).

[46] Y. Lin, Q. Zeng, W. Yang, and W. L. Mao, Pressure-induced densification in GeO_2 glass: A transmission x-ray microscopy study, Appl. Phys. Lett. **103**, 261909 (2013).

[47] R. J. Angel, J. Gonzalez-Platas, and M. Alvaro, EosFit7c and a Fortran module (library) for equation of state calculations, Z. Kristallogr. - Cryst. Mater. **229**, 405 (2014).

[48] X. Hong, G. Shen, V. B. Prakapenka, M. Newville, M. L. Rivers, and S. R. Sutton, Intermediate states of GeO_2 glass under pressures up to 35 GPa, Phys. Rev. B **75**, 104201 (2007).

[49] Y. Kuwayama, K. Hirose, N. Sata, and Y. Ohishi, The pyrite-type high-pressure form of silica, Science **309**, 923 (2005).

[50] Y. Kuwayama, K. Hirose, N. Sata, and Y. Ohishi, Pressure-induced structural evolution of pyrite-type SiO_2, Phys. Chem. Miner. **38**, 591 (2011).

[51] H. Dekura, T. Tsuchiya, and J. Tsuchiya, First-principles prediction of post-pyrite phase transitions in germanium dioxide, Phys. Rev. B **83**, 134114 (2011).

[52] S. Wu, K. Umemoto, M. Ji, C.-Z. Wang, K.-M. Ho, and R. M. Wentzcovitch, Identification of post-pyrite phase transitions in SiO_2 by a genetic algorithm, Phys. Rev. B **83**, 184102 (2011).

[53] D. Nishio-Hamane, A. Shimizu, R. Nakahira, K. Niwa, A. Sano-Furukawa, T. Okada, T. Yagi, and T. Kikegawa, The stability and equation of state for the cotunnite phase of TiO_2 up to 70 GPa, Phys. Chem. Miner. **37**, 129 (2010).

[54] V. Swamy and B. C. Muddle, Ultrastiff Cubic TiO_2 Identified via First-Principles Calculations, Phys. Rev. Lett. **98**, 035502 (2007).

[55] N. Dubrovinskaia, L. S. Dubrovinsky, R. Ahuja, V. B. Prokopenko, V. Dmitriev, H. P. Weber, J. M. Osorio-Guillen, and B. Johansson, Experimental and Theoretical Identification of a New High-Pressure TiO_2 Polymorph, Phys. Rev. Lett. **87**, 275501 (2001).

[56] Y. Kono, Y. Shibazaki, C. Kenney-Benson, Y. Wang, and G. Shen, Pressure-induced structural change in $MgSiO_3$ glass at pressures near the Earth's core–mantle boundary, Proc. Natl. Acad. Sci. USA **115**, 1742 (2018).

[57] A. Denoeud, S. Mazevet, F. Guyot, F. Dorchies, J. Gaudin, A. Ravasio, E. Brambrink, and A. Benuzzi-Mounaix, High-pressure structural changes in liquid silica, Phys. Rev. E **94**, 031201 (2016).

[58] L. Stixrude, N. de Koker, N. Sun, M. Mookherjee, and B. B. Karki, Thermodynamics of silicate liquids in the deep Earth, Earth Planet. Sci. Lett. **278**, 226 (2009).

[59] B. B. Karki, D. B. Ghosh, C. Maharjan, S. Karato, and J. Park, Density-pressure profiles of Fe-bearing $MgSiO_3$ liquid: Effects of valence and spin states, and implications for the chemical evolution of the lower mantle, Geophys. Res. Lett. **45**, 3959 (2018).

[60] D. Andrault, S. Petitgirard, G. Lo Nigro, J.-L. Devidal, G. Veronesi, G. Garbarino, and M. Mezouar, Solid-liquid iron partitioning in Earth's deep mantle, Nature **487**, 354 (2012).

[61] R. Nomura, H. Ozawa, S. Tateno, K. Hirose, J. Hernlund, S. Muto, H. Ishii, and N. Hiraoka, Spin crossover and iron-rich silicate melt in the Earth's deep mantle, Nature **473**, 199 (2011).